

## Softening and Residual Loss Modulus of Jammed Grains under Oscillatory Shear in an Absorbing State

Michio Otsuki<sup>\*</sup>

*Graduate School of Engineering Science, Osaka University, Toyonaka, Osaka 560-8531, Japan*

Hisao Hayakawa<sup>Ⓜ</sup>

*Yukawa Institute for Theoretical Physics, Kyoto University, Kitashirakawaiwake-cho, Sakyo-ku, Kyoto 606-8502, Japan*



(Received 21 January 2021; revised 26 December 2021; accepted 22 April 2022; published 17 May 2022)

From a theoretical study of the mechanical response of jammed materials comprising frictionless and overdamped particles under oscillatory shear, we find that the material becomes soft, and the loss modulus remains nonzero even in an absorbing state where any irreversible plastic deformation does not exist. The trajectories of the particles in this region exhibit hysteresis loops. We succeed in clarifying the origin of the softening of the material and the residual loss modulus with the aid of Fourier analysis. We also clarify the roles of the yielding point in the softening to distinguish the plastic deformation from reversible deformation in the absorbing state.

DOI: [10.1103/PhysRevLett.128.208002](https://doi.org/10.1103/PhysRevLett.128.208002)

**Introduction.**—The mechanical response of jammed disordered materials, such as granular materials, foams, emulsions, and colloidal suspensions, garners much attention [1,2]. For vanishingly small strain, the shear stress  $\sigma$  is proportional to the shear strain  $\gamma$ , which is characterized by the shear modulus satisfying a critical scaling law near the jamming point  $\phi_J$  [3–5]. However, the region of the linear response is quite narrow near  $\phi_J$  [6,7]. Hence, revealing the nonlinear response is essential for understanding the dynamics of disordered materials.

In crystalline materials, the nonlinear response originates from yielding associated with irreversible plastic deformation. Yielding also takes place in disordered materials when the strain is sufficiently large [8–13]. The yielding transition attracts much attention among researchers as an example of the reversible-irreversible transition [14–17]. When plastic deformation causes rearrangements of contact networks, the mechanical response becomes nonlinear. It had been believed that plastic deformation is always necessary for the nonlinear response. Unlike this expectation, recent studies have revealed that plastic deformation is not always necessary for the nonlinear response [18–22]. Under steady shear,  $\sigma$  becomes hypoelastic before the yielding [18,20], and the storage modulus in the steady state after applying a sufficient number of cyclic shears decreases as the strain amplitude increases without any irreversible plastic deformation [21]. The decrease of the storage modulus is called softening.

It is known that plastic deformation causes dissipation characterized by the loss modulus [21,22]. It is natural that the loss modulus disappears in quasistatic strains without any plastic deformation. However, we need a careful check of this naive picture, because the loss modulus might be

related to the softening observed without any plastic deformation.

The mechanical response should be related to the motion of particles constituting the disordered materials. This suggests that the trajectories of particles provide information on the softening of the materials. Several studies have reported that the trajectories of dense particles form closed loops under oscillatory shear below the yielding point associated with reversible contact changes where there are some cyclic open and closed contacts between particles [23–34]. The formation of closed loops means that the system is reduced to an absorbing state after some time has passed. A previous study numerically showed that the softening in the absorbing state becomes significant when there are closed loops associated with many contact changes. However, the quantitative relationship remains unclear [21].

In this Letter, we numerically investigate jammed materials comprising  $N$  frictionless and overdamped particles under oscillatory shear to clarify the origin of the softening. For this purpose, we focus on the roles of the trajectories to clarify the relationship between the softening in the absorbing state and the softening in the plastic regime. We find that the shear modulus exhibits softening, and the loss modulus remains nonzero even in the absorbing state below the yielding point. The trajectory of a test particle forms a nontrivial loop in this region. With the aid of Fourier analysis, we investigate the geometric structure of the trajectories and reveal the role of Fourier components for the storage and loss moduli. We also present the theoretical expressions for the storage and loss moduli, whose quantitative validities are numerically confirmed.

**Setup.**—Let us consider a jammed two-dimensional system consisting of frictionless particles under oscillatory

shear. The particles are driven by the overdamped equation with Stokes' drag under Lees-Edwards boundary conditions [35], where the equation of motion is given by

$$\zeta \left\{ \frac{d}{dt} \mathbf{r}_i - \dot{\gamma}(t) y_i \mathbf{e}_x \right\} = - \sum_{j \neq i} \frac{\partial}{\partial \mathbf{r}_i} U(r_{ij}), \quad (1)$$

with the position  $\mathbf{r}_i = (x_i, y_i)$  of particle  $i$ . Here,  $\zeta$  and  $\dot{\gamma}(t)$  are the drag coefficient and strain rate, respectively. The interaction potential  $U(r_{ij})$  is assumed to be

$$U(r_{ij}) = \frac{k}{2} (d_{ij} - r_{ij})^2 \Theta(d_{ij} - r_{ij}), \quad (2)$$

where  $\Theta(x)$ ,  $k$ ,  $d_{ij}$ , and  $r_{ij} = |\mathbf{r}_{ij}| = |\mathbf{r}_i - \mathbf{r}_j|$  are the Heaviside step function satisfying  $\Theta(x) = 1$  for  $x \geq 0$  and  $\Theta(x) = 0$  otherwise, the spring constant, the average diameter of particles  $i$  and  $j$ , and the distance between particles  $i$  and  $j$ , respectively. The system is bidisperse and consists of an equal number of particles with diameters  $d_0$  and  $d_0/1.4$ . We have verified that particles with inertia and damping at contact, which corresponds to the model in Ref. [21], exhibit almost identical behavior in our system [36].

We prepare the initial state with a given packing fraction  $\phi$  by slowly compressing the system from a state below the jamming point  $\phi_J \simeq 0.841$  [5]. The oscillatory shear strain is applied for  $n_c$  cycles as

$$\gamma(\theta) = \gamma_0 \sin \theta \quad (3)$$

with the phase  $\theta = \omega t$ , where  $\gamma_0$  and  $\omega$  are the strain amplitude and angular frequency, respectively. Note that the shear rate satisfies  $\dot{\gamma}(t) = (d\theta/dt)(d/d\theta)\gamma(\theta)$ . In the last cycle, we measure the storage and loss moduli  $G'$  and  $G''$ , respectively, given by [37]

$$G' = \frac{1}{\pi} \int_0^{2\pi} d\theta \frac{\langle \sigma(\theta) \rangle \sin \theta}{\gamma_0}, \quad (4)$$

$$G'' = \frac{1}{\pi} \int_0^{2\pi} d\theta \frac{\langle \sigma(\theta) \rangle \cos \theta}{\gamma_0}, \quad (5)$$

with shear stress

$$\sigma = \frac{1}{L^2} \sum_i \sum_{j>i} \frac{x_{ij} y_{ij}}{r_{ij}} U'(r_{ij}), \quad (6)$$

where  $x_{ij} = x_i - x_j$ ,  $y_{ij} = y_i - y_j$ , and  $\langle \cdot \rangle$  represents the ensemble average, and  $L$  is the linear system size. See Ref. [36] for the stress-strain curves in our system. We have verified that  $G'$  and  $G''$  are independent of  $N$  and  $n_c$  for  $N \geq 1000$  and  $n_c \geq 20$  [36]. We use  $N = 1000$  and  $n_c = 20$  in our numerical analysis. We adopt the Euler method using the time step  $\Delta t = 0.05\tau_0$  with  $\tau_0 = \zeta/k$ .

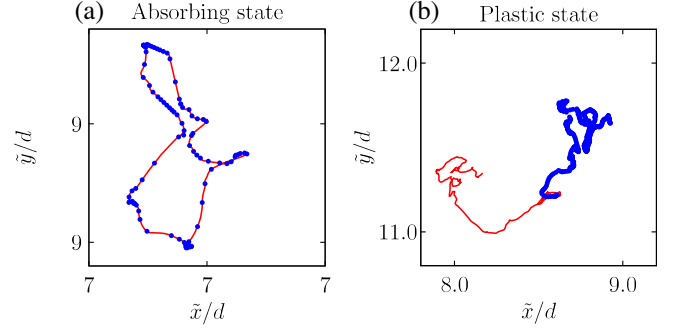


FIG. 1. Nonaffine particle trajectories in the last two cycles for  $\gamma_0 = 0.02$  (a) and  $0.1$  (b) with  $\omega = 10^{-4}\tau_0^{-1}$  and  $\phi = 0.87$ , which corresponds to  $\phi - \phi_J = 0.029$ . The circles represent the trajectory in the last cycle. The line represents the trajectory in the second to the last cycle.

*Closed trajectories.*—As the number of cycles increases, the system reaches a statistically steady state through a transient regime as shown in Ref. [36]. Figure 1 displays typical nonaffine trajectories of a particle

$$\tilde{\mathbf{r}}_i(\theta) = \mathbf{r}_i(\theta) - \gamma(\theta) y_i(\theta) \mathbf{e}_x \quad (7)$$

in the last two cycles with  $\phi = 0.87$  and  $\omega = 10^{-4}\tau_0^{-1}$  in the steady state. In Fig. 1(a) ( $\gamma_0 = 0.02$ ), the trajectories are closed, and the particle returns to its original position after every cycle. This indicates that irreversible plastic deformation does not occur, at least in the last two cycles. The closed trajectories form nontrivial loops, which differ from ellipses or lines observed for small  $\gamma_0$  as shown in Ref. [36]. In Fig. 1(b) ( $\gamma_0 = 0.1$ ), the particle moves away from its original positions after a cycle, as a characteristic behavior of plastic deformation. Here, we define the absorbing state where the displacement of each particle after several cycles is smaller than  $d_c = 10^{-4}d_0$  in the statistically steady state. We also define the plastic state where the displacement after several cycles exceeds  $d_c$ . It should be noted that some rare samples exhibit trajectories where particles return to their original positions after more than one cycle [27,28,30,31,33]. However, our theoretical results shown below are unchanged even if such samples exist [36].

*Shear modulus.*—We plot the storage modulus  $G'$  against the strain amplitude  $\gamma_0$  for  $\omega = 10^{-4}\tau_0^{-1}$  with  $\phi = 0.870, 0.860, 0.850,$  and  $0.845$  in Fig. 2. The yielding points to distinguish the absorbing state from the plastic state for various  $\phi$  are shown by open pentagons [36]. The storage modulus  $G'$  decreases as  $\gamma_0$  increases, but the yielding point is not identical to the point where  $G'$  starts to decrease. We call the decrease for  $\gamma_0 < \gamma_c$ , the yielding strain amplitude, the softening in the absorbing state (SAS). We also call the decrease for  $\gamma_0 > \gamma_c$  the softening in the plastic state (SPS). It is remarkable that SAS is continuously connected to SPS, while a shoulder in  $G'$  appears in SPS for  $0.04 \leq \gamma_0 \leq 0.1$  with  $\phi = 0.845$ . In the inset of Fig. 2, we demonstrate that

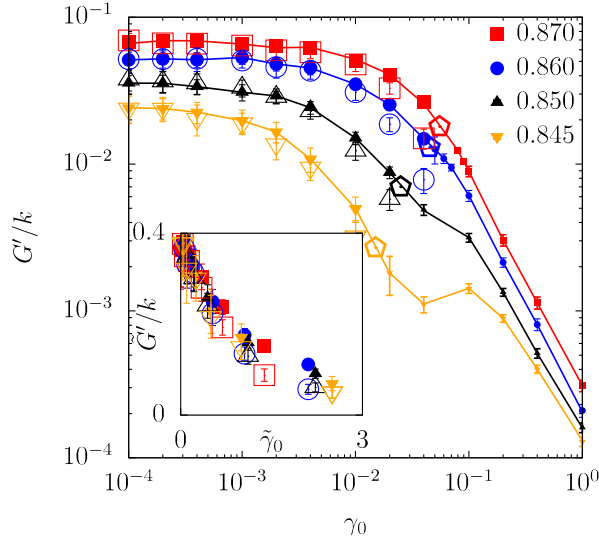


FIG. 2. Storage modulus  $G'$  obtained in our simulation (filled symbols) against  $\gamma_0$  for  $\omega = 10^{-4}\tau_0^{-1}$  with  $\phi = 0.870, 0.860, 0.850,$  and  $0.845$ , which corresponds to  $\phi - \phi_J = 0.029, 0.019, 0.009,$  and  $0.004$ , respectively. The legends represent the packing fraction  $\phi$ . The data in the absorbing (plastic) state obtained in our simulation are shown in smaller (larger) filled symbols. The open pentagons represent the yielding strain amplitude  $\gamma_c$ , while other open symbols represent the theoretical expression using  $G'_T$  in Eq. (14). (Inset) Scaled storage modulus  $\tilde{G}' = G'/\sqrt{\phi - \phi_J}$  obtained in our simulation (filled symbols) and its theoretical expression using  $G'_T$  (open symbols) in Eq. (14) against scaled strain amplitude  $\tilde{\gamma}_0 = \gamma_0/(\phi - \phi_J)$  in the absorbing state.

$G'$  and  $\gamma_0$  can be scaled by  $\sqrt{\phi - \phi_J}$  and  $\phi - \phi_J$ , respectively, as indicated in Refs. [3,21]. We have confirmed that  $G'$  is independent of  $\omega$  for  $\omega \leq 10^{-3}\tau_0^{-1}$ .

Figure 3(a) displays the loss modulus  $G''$  in the absorbing state against  $\gamma_0$  for  $\omega = 10^{-4}\tau_0^{-1}$  with  $\phi = 0.870, 0.860, 0.850,$  and  $0.845$ , in which  $G''$  does not strongly depend on  $\phi$  and  $\gamma_0$ . See Ref. [36] for  $G''$  in the plastic state. In Fig. 3(b), we plot the loss modulus  $G''$  in the absorbing state against  $\omega$  for  $\phi = 0.87$  with  $\gamma = 0.01$ . Remarkably,  $G''$  in Fig. 3(b) seems to converge to a nonzero value in the limit  $\omega \rightarrow 0$ , which contrasts with the behavior of the Kelvin-Voigt model (i.e.,  $G'' \propto \omega$  [38]). This behavior indicates that dissipation remains even in the quasistatic limit in the absorbing state. Note that  $G'' \propto \omega$  is recovered when we adopt a sufficiently small  $\gamma_0$  [36].

*Fourier analysis.*—In the absorbing state, the nonaffine trajectory  $\tilde{\mathbf{r}}_i(\theta)$  of particle  $i$  can be expressed in a Fourier series as

$$\tilde{\mathbf{r}}_i(\theta) = \mathbf{R}_i + \sum_{n=1}^{\infty} (\mathbf{a}_i^{(n)} \sin n\theta + \mathbf{b}_i^{(n)} \cos n\theta), \quad (8)$$

with the center of the trajectory

$$\mathbf{R}_i = (X_i, Y_i) = \frac{1}{2\pi} \int_0^{2\pi} d\theta \tilde{\mathbf{r}}_i(\theta), \quad (9)$$

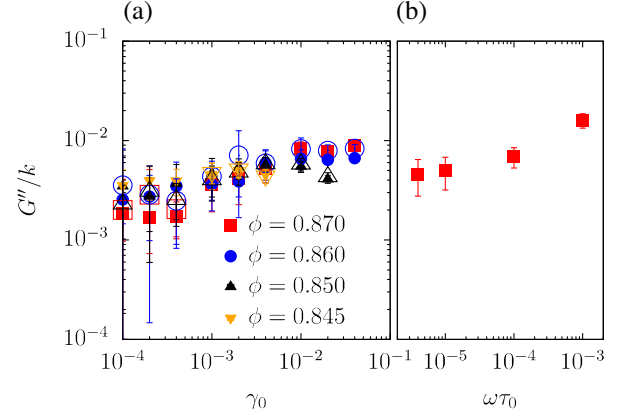


FIG. 3. (a) Loss modulus  $G''$  in the absorbing state obtained in our simulation (filled symbols) and its theoretical expression  $G''_T$  (open symbols) in Eq. (15) against  $\gamma_0$  for  $\omega = 10^{-4}\tau_0^{-1}$  with  $\phi = 0.870, 0.860, 0.850,$  and  $0.845$ , which corresponds to  $\phi - \phi_J = 0.029, 0.019, 0.009,$  and  $0.004$ , respectively. (b) Loss modulus  $G''$  against  $\omega\tau_0$  for  $\phi = 0.87$  with  $\gamma_0 = 0.01$ .

and the Fourier coefficients

$$\mathbf{a}_i^{(n)} = \frac{1}{\pi} \int_0^{2\pi} d\theta \sin n\theta \tilde{\mathbf{r}}_i(\theta), \quad (10)$$

$$\mathbf{b}_i^{(n)} = \frac{1}{\pi} \int_0^{2\pi} d\theta \cos n\theta \tilde{\mathbf{r}}_i(\theta). \quad (11)$$

If  $\mathbf{a}_i^{(n)} = \mathbf{b}_i^{(n)} = \mathbf{0}$  for all  $n$ , the particle motion is affine. When only  $\mathbf{a}_i^{(1)}$  is nonzero, the nonaffine trajectory is a straight line, as shown in Fig. 4(a). In contrast, the trajectory exhibits an ellipse when  $\mathbf{b}_i^{(1)}$  is also nonzero, as shown in Fig. 4(b). A nontrivial trajectory, as shown in Fig. 1(a), contains modes with  $n \geq 2$ . See Ref. [36] for the relationship between the trajectories and the Fourier coefficients.

In Fig. 5(a), we plot the magnitudes of the Fourier components

$$a^{(n)} = \sum_i \langle |\mathbf{a}_i^{(n)}| \rangle / N, \quad b^{(n)} = \sum_i \langle |\mathbf{b}_i^{(n)}| \rangle / N, \quad (12)$$

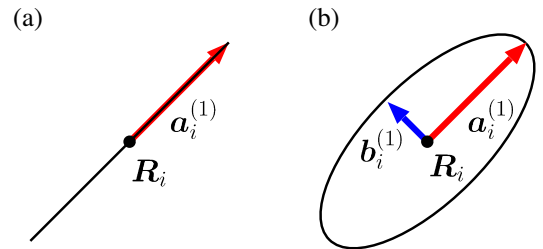


FIG. 4. Schematics of the nonaffine trajectory when only  $\mathbf{a}_i^{(1)}$  is nonzero (a) and only  $\mathbf{a}_i^{(1)}$  and  $\mathbf{b}_i^{(1)}$  are nonzero (b).

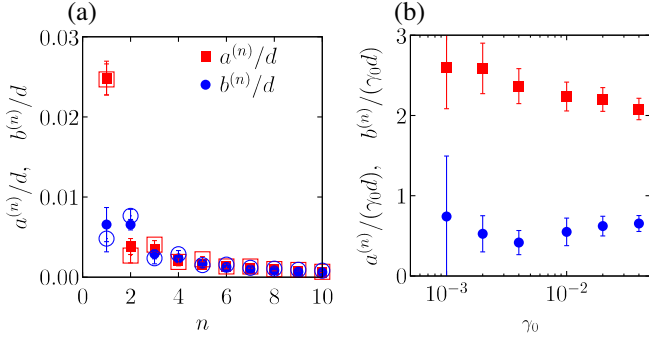


FIG. 5. (a) Magnitudes of Fourier coefficients  $a^{(n)}$  and  $b^{(n)}$  against  $n$  for  $\phi = 0.87$  and  $\gamma_0 = 0.02$  with  $\omega\tau_0 = 10^{-4}$  (filled symbols) and  $10^{-5}$  (open symbols). (b) Magnitudes of the Fourier coefficients  $a^{(n)}$  and  $b^{(n)}$  normalized by  $\gamma_0$  against  $\gamma_0$  for  $\phi = 0.87$  and  $\omega\tau_0 = 10^{-4}$  with  $n = 1$ .  $\phi = 0.87$  corresponds to  $\phi - \phi_J = 0.029$ .

obtained from our numerical data using Eqs. (10) and (11) against  $n$  for  $\phi = 0.87$  and  $\gamma_0 = 0.01$  with  $\omega\tau_0 = 10^{-4}$  and  $10^{-5}$ . The Fourier components do not strongly depend on  $\omega$ , which indicates that the nontrivial loops do not disappear in the limit  $\omega \rightarrow 0$ . For different  $\phi > \phi_J$  and  $\gamma_0 \geq 10^{-3}$ , we have confirmed that  $a^{(1)}$  is always the largest [39], the other modes are nonzero to make loops with nonzero areas, and the Fourier components are independent of  $\omega$ . In Fig. 5(b), we plot  $a^{(n)}/\gamma_0$  and  $b^{(n)}/\gamma_0$  against  $\gamma_0$  for  $\phi = 0.87$  and  $\omega\tau_0 = 10^{-4}$  with  $n = 1$ , where  $a^{(n)}/\gamma_0$  and  $b^{(n)}/\gamma_0$  are almost independent of  $\gamma_0$ . This behavior is consistent with that for the number of contact changes [36].

*Theoretical analysis.*—Now, let us reproduce the numerical results by a simple analytic calculation. Substituting Eq. (8) into Eq. (7),  $\mathbf{r}_{ij}(\theta)$  is given by

$$\mathbf{r}_{ij}(\theta) = \mathbf{R}_{ij} + \gamma_0 Y_{ij} \sin \theta \mathbf{e}_x + \sum_{n=1}^{\infty} (a_{ij}^{(n)} \sin n\theta + b_{ij}^{(n)} \cos n\theta). \quad (13)$$

Here, we define  $\mathbf{a}_{ij}^{(n)} = \mathbf{a}_i^{(n)} - \mathbf{a}_j^{(n)}$ ,  $\mathbf{b}_{ij}^{(n)} = \mathbf{b}_i^{(n)} - \mathbf{b}_j^{(n)}$ , and  $\mathbf{R}_{ij} = (X_{ij}, Y_{ij}) = \mathbf{R}_i - \mathbf{R}_j$ . Substituting Eq. (13) into Eq. (4) with Eq. (6) and neglecting the terms of  $\mathcal{O}(\gamma_0)$ , we obtain the expression  $G_T'$  of the storage modulus in SAS as [36]

$$\begin{aligned} G_T' = & -\frac{1}{L^2} \sum_{ij} \left\langle \frac{X_{ij}^2 Y_{ij}^2}{R_{ij}^2} \Psi'(R_{ij}) \right\rangle - \frac{1}{L^2} \sum_{ij} \langle Y_{ij}^2 \Psi(R_{ij}) \rangle \\ & - \frac{1}{L^2} \sum_{ij} \left\langle \left( \frac{a_{ij,x}^{(1)}}{\gamma_0} Y_{ij} + X_{ij} \frac{a_{ij,y}^{(1)}}{\gamma_0} \right) \Psi(R_{ij}) \right\rangle \\ & - \frac{1}{L^2} \sum_{ij} \left\langle X_{ij} Y_{ij} \Psi'(R_{ij}) \frac{\mathbf{R}_{ij} \cdot \mathbf{a}_{ij}^{(1)}}{\gamma_0 R_{ij}} \right\rangle, \end{aligned} \quad (14)$$

where  $\Psi(r) = -U'(r)/r$ . Here, we have assumed  $|\mathbf{a}_i^{(n)}| \sim |\mathbf{b}_i^{(n)}| \sim \gamma_0$  and  $\gamma_0 \ll 1$ . In the expression of Eq. (14), only the first harmonic contribution from  $\mathbf{a}_i^{(1)}$  can survive because of Eq. (5). Note that  $\mathbf{R}_i$  and  $\mathbf{a}_i^{(1)}$  cannot be determined within the theory but are determined by our simulation data. In Fig. 2, we plot the theoretical prediction  $G_T'$  as open symbols. The theoretical prediction quantitatively reproduces the numerical results except for large  $\gamma_0$ , which is out of the scope of our theory. The first and second terms on the right-hand side (rhs) of Eq. (14) represent the contributions from the affine transformation depending only on  $\mathbf{R}_i$ , while the third and fourth terms including  $\mathbf{a}_{ij}^{(1)}/\gamma_0$  indicate the contributions from the nonaffine trajectories. As shown in Ref. [36], the contributions from the nonaffine trajectories are almost independent of  $\gamma_0$ , which is consistent with the behavior of  $a^{(1)}/\gamma_0$  shown in Fig. 5(b). Numerical evaluation in Ref. [36] reveals that SAS is dominated by the first term on rhs of Eq. (14) through the change of  $\mathbf{R}_i$ . The center of the nonaffine trajectories  $\mathbf{R}_i$  is changed by the rearrangement of the configuration during the transient to the absorbing state, which is consistent with the memory formation of dense particles during oscillatory shear [40–42].

The theoretical expression  $G_T''$  of the loss modulus in SAS is given by [36]

$$\begin{aligned} G_T'' = & -\frac{1}{L^2} \sum_{ij} \left\langle \left( \frac{b_{ij,x}^{(1)}}{\gamma_0} Y_{ij} + X_{ij} \frac{b_{ij,y}^{(1)}}{\gamma_0} \right) \Psi(R_{ij}) \right\rangle \\ & - \frac{1}{L^2} \sum_{ij} \left\langle X_{ij} Y_{ij} \Psi'(R_{ij}) \frac{\mathbf{R}_{ij} \cdot \mathbf{b}_{ij}^{(1)}}{\gamma_0 R_{ij}^2} \right\rangle, \end{aligned} \quad (15)$$

where we have used the same assumption to obtain Eq. (14). Similar to the case of  $G_T'$ , only the contribution of the first harmonics  $\mathbf{b}_i^{(1)}$  in the expression of Eq. (8) can survive because of Eq. (5). Note that  $\mathbf{b}_i^{(1)}$  cannot be determined within the theory but is evaluated by the simulation data. The loss modulus depends only on the nonaffine contribution including  $\mathbf{b}_i^{(1)}$ . The amplitude  $b^{(1)}$  remains nonzero in the limit  $\omega \rightarrow 0$ , which leads to the residual loss modulus as in Fig. 3(b). We plot the theoretical expression  $G_T''$  using the open symbols in Fig. 3(a).  $G_T''$  also reproduces the numerical results except for large  $\gamma_0$ . Thus, our theory reveals the quantitative relationship between the loss modulus and closed trajectories, which was suggested in Ref. [26].

*Conclusion.*—We numerically studied the mechanical response of jammed materials consisting of frictionless and overdamped particles under oscillatory shear. The shear modulus exhibits SAS and the residual loss modulus exists in the quasi-static limit in the absorbing state. Through Fourier analysis of the closed trajectories, the theoretical

expressions for the storage and loss moduli quantitatively agree with the numerical results.

Reference [4] reported that the loss modulus vanishes in the absorbing jammed states in the limit  $\omega \rightarrow 0$ , which is inconsistent with our result. It is noteworthy that Ref. [4] did not consider any transient state associated with contact changes before the system reaches the absorbing state. Since the loss modulus is expected to be given by the generalized Green-Kubo formula [43,44], the origin of the residual loss modulus might be plastic events in the transient dynamics.

Recent studies of large amplitude oscillatory shear (LAOS) reveal that there are contributions from higher harmonics in the mechanical response of nonlinear viscoelastic materials [45,46]. We calculate nonlinear viscoelastic moduli  $G'_n$  and  $G''_n$  with  $n \geq 2$  and confirm that such higher order moduli are negligible in our system as shown in Ref. [36].

In this Letter, we focus only on the nonlinear response of disordered frictionless particles. However, even frictional grains and exhibit SAS depending on the friction coefficient [47]. Therefore, an extension of our theory to these systems will be our future work.

The authors thank K. Saitoh, D. Ishima, T. Kawasaki, K. Miyazaki, and K. Takeuchi for fruitful discussions. This work was supported by JSPS KAKENHI Grants No. JP16H04025, No. JP21H01006, and No. JP19K03670 and ISHIZUE 2020 of the Kyoto University Research Development Program.

---

\*otsuki@me.es.osaka-u.ac.jp

- [1] M. van Hecke, *J. Phys. Condens. Matter* **22**, 033101 (2010).
- [2] R. P. Behringer and B. Chakraborty, *Rep. Prog. Phys.* **82**, 012601 (2019).
- [3] C. S. O'Hern, S. A. Langer, A. J. Liu, and S. R. Nagel, *Phys. Rev. Lett.* **88**, 075507 (2002).
- [4] B. P. Tighe, *Phys. Rev. Lett.* **107**, 158303 (2011).
- [5] M. Otsuki and H. Hayakawa, *Phys. Rev. E* **95**, 062902 (2017).
- [6] C. Coulais, A. Seguin, and O. Dauchot, *Phys. Rev. Lett.* **113**, 198001 (2014).
- [7] M. Otsuki and H. Hayakawa, *Phys. Rev. E* **90**, 042202 (2014).
- [8] K. Hima Nagamanasa, S. Gokhale, A. K. Sood, and R. Ganapathy, *Phys. Rev. E* **89**, 062308 (2014).
- [9] E. D. Knowlton, D. J. Pine, and L. Cipelletti, *Soft Matter* **10**, 6931 (2014).
- [10] T. Kawasaki and L. Berthier, *Phys. Rev. E* **94**, 022615 (2016).
- [11] P. Leishangthem, A. D. S. Parmar, and S. Sastry, *Nat. Commun.* **8**, 14653 (2017).
- [12] A. H. Clark, J. D. Thompson, M. D. Shattuck, N. T. Ouellette, and C. S. O'Hern, *Phys. Rev. E* **97**, 062901 (2018).
- [13] J. Boschan, S. Luding, and B. P. Tighe, *Granular Matter* **21**, 58 (2019).
- [14] H. Hinrichsen, *Adv. Phys.* **49**, 815 (2000).
- [15] M. Henkel, H. Hinrichsen, and S. Lubeck, *Non-Equilibrium Phase Transition I: Absorbing Phase Transitions* (Springer, Heidelberg, 2008).
- [16] D. J. Pine, J. P. Collub, J. F. Brady, and A. M. Leshansky, *Nature (London)* **438**, 997 (2005).
- [17] L. Cort e, P. M. Chaikin, J. P. Gollub, and D. J. Pine, *Nat. Phys.* **4**, 420 (2008).
- [18] J. Boschan, D. Vågberg, E. Somfai, and B. P. Tighe, *Soft Matter* **12**, 5450 (2016).
- [19] D. Nakayama, H. Yoshino, and F. Zamponi, *J. Stat. Mech.* (2016) 104001.
- [20] T. Kawasaki and K. Miyazaki, *arXiv:2003.10716*.
- [21] S. Dagois-Bohy, E. Somfai, B. P. Tighe, and M. van Hecke, *Soft Matter* **13**, 9036 (2017).
- [22] D. Ishima and H. Hayakawa, *Phys. Rev. E* **101**, 042902 (2020).
- [23] M. Lundberg, K. Krishan, N. Xu, C. S. O'Hern, and M. Dennin, *Phys. Rev. E* **77**, 041505 (2008).
- [24] C. F. Schreck, R. S. Hoy, M. D. Shattuck, and C. S. O'Hern, *Phys. Rev. E* **88**, 052205 (2013).
- [25] N. C. Keim and P. E. Arratia, *Soft Matter* **9**, 6222 (2013).
- [26] N. C. Keim and P. E. Arratia, *Phys. Rev. Lett.* **112**, 028302 (2014).
- [27] I. Regev, T. Lookman, and C. Reichhardt, *Phys. Rev. E* **88**, 062401 (2013).
- [28] I. Regev, J. Weber, C. Reichhardt, K. A. Dahmen, and T. Lookman, *Nat. Commun.* **6**, 8805 (2015).
- [29] N. V. Priezjev, *Phys. Rev. E* **93**, 013001 (2016).
- [30] M. O. Lavrentovich, A. J. Liu, and S. R. Nagel, *Phys. Rev. E* **96**, 020101(R) (2017).
- [31] K. Nagasawa, K. Miyazaki, and T. Kawasaki, *Soft Matter* **15**, 7557 (2019).
- [32] P. Das, H. A. Vinutha, and S. Sastry, *Proc. Natl. Acad. Sci. U.S.A.* **117**, 10203 (2020).
- [33] K. Khirallah, B. Tyukodi, D. Vandembroucq, and C. E. Maloney, *Phys. Rev. Lett.* **126**, 218005 (2021).
- [34] M. S. van Deen, J. Simon, Z. Zeravcic, S. Dagois-Bohy, B. P. Tighe, and M. van Hecke, *Phys. Rev. E* **90**, 020202(R) (2014).
- [35] D. J. Evans and G. P. Morriss, *Statistical Mechanics of Nonequilibrium Liquids*, 2nd ed. (Cambridge University Press, Cambridge, 2008).
- [36] See Supplemental Material at <http://link.aps.org/supplemental/10.1103/PhysRevLett.128.208002> for some details not written in the main text.
- [37] M. Doi and S. F. Edwards, *The Theory of Polymer Dynamics* (Oxford University Press, Oxford, 1986).
- [38] M. Meyers and K. Chawla, *Mechanical Behavior of Materials* (Cambridge University Press, Cambridge, England, 2008).
- [39] We suppose  $a^{(1)}$  is the largest because the mode proportional to  $a^{(1)}$  is synchronized with the external oscillation  $\sin \theta$ .
- [40] D. Fiocco, G. Foffi, and S. Sastry, *Phys. Rev. Lett.* **112**, 025702 (2014).
- [41] J. D. Paulsen, N. C. Keim, and S. R. Nagel, *Phys. Rev. Lett.* **113**, 068301 (2014).
- [42] M. Adhikari and S. Sastry, *Eur. Phys. J. E* **41**, 105 (2018).

- [43] S-H. Chong, M. Otsuki, and H. Hayakawa, *Phys. Rev. E* **81**, 041130 (2010).
- [44] H. Hayakawa and M. Otsuki, *Phys. Rev. E* **88**, 032117 (2013).
- [45] M.H. Wagner, V.H. Rolón-Garrido, K. Hyun, and M. Wilhelm, *J. Rheol.* **55**, 495 (2011).
- [46] K. Hyun, M. Wilhelm, C. O. Klein, K. S. Cho, J. G. Nam, K. H. Ahn, S. J. Lee, R. H. Ewoldt, and G. H. McKinley, *Prog. Polym. Sci.* **36**, 1697 (2011).
- [47] M. Otsuki and H. Hayakawa, *Eur. Phys. J. E* **44**, 70 (2021).